Materials Today Advances 19 (2023) 100408

Contents lists available at ScienceDirect

Materials Today Advances

journal homepage: www.journals.elsevier.com/materials-today-advances/

Inkjet-printed morphogenesis of tumor-stroma interface using bi-cellular bioinks of collagen-poly(N-isopropyl acrylamide-co-methyl methacrylate) mixture

Cih Cheng [a], Naomi Deneke [b], Hye-ran Moon [a], Sae Rome Choi [a], Natalia Ospina-Muñoz [a], Bennett D. Elzey [c,e], Chelsea S. Davis [b], George T.-C Chiu [a], Bumsoo Han [a,c,d,*]

[a] School of Mechanical Engineering, Purdue University, West Lafayette, IN, USA
[b] School of Materials Engineering, Purdue University, West Lafayette, IN, USA
[c] Purdue Institute for Cancer Research, Purdue University, West Lafayette, IN, USA
[d] Weldon School of Biomedical Engineering, Purdue University, West Lafayette, IN, USA
[e] Department of Comparative Pathobiology, Purdue University, West Lafayette, IN, USA

ARTICLE INFO

Keywords:
Tumoroids
Cancer-associated fibroblasts
Cell-derived contraction
Interpenetrating polymer network
3D printing

ABSTRACT

Recent advances in biomaterials and 3D printing/culture methods enable various tissue-engineered tumor models. However, it is still challenging to achieve native tumor-like characteristics due to lower cell density than native tissues and prolonged culture duration for maturation. Here, we report a new method to create tumoroids with a mechanically active tumor-stroma interface at extremely high cell density. This method, named "inkjet-printed morphogenesis" (iPM) of the tumor-stroma interface, is based on a hypothesis that cellular contractile force can significantly remodel the cell-laden polymer matrix to form densely-packed tissue-like constructs. Thus, differential cell-derived compaction of tumor cells and cancer-associated fibroblasts (CAFs) can be used to build a mechanically active tumor-stroma interface. In this methods, two kinds of bioinks are prepared, in which tumor cells and CAFs are suspended respectively in the mixture of collagen and poly (N-isopropyl acrylamide-co-methyl methacrylate) solution. These two cellular inks are inkjet-printed in multi-line or multi-layer patterns. As a result of cell-derived compaction, the resulting structure forms tumoroids with mechanically active tumor-stroma interface at extremely high cell density. We further test our working hypothesis that the morphogenesis can be controlled by manipulating the force balance between cellular contractile force and matrix stiffness. Furthermore, this new concept of "morphogenetic printing" is demonstrated to create more complex structures beyond current 3D bioprinting techniques.

1. Introduction

Tissues are complex structures made up from different cell types embedded in extracellular matrix, generating a three dimensional structure (3D). Being able to generate 3D tissue outside the body that resembles some characteristics of the tissue *in vivo* is a fascinating field [1]. Three-dimensional engineered tumor models emerge as new tool for cancer biology, drug discovery, and medical research [2–7]. These models include spheroids, organoids, microfluidic platforms, and 3D-printed constructs [3,8–11]. Among the models, spheroids and organoids are the most commonly used models for cancer research [12, 13]. These two models have overlapping purposes but differ in cellular sources and preparation protocols. Spheroids are of lower complexity but capable of recapitulating several features of the 3D tumor micro-environment: structural organization, cellular layered assembling, hypoxia, and nutrient/oxygen gradients [14]. Techniques to prepare spheroids include hanging drop methods, formation on low-attachment surfaces, magnetic levitation, spinner flasks, and matrix encapsulation [15]. On the other hand, organoids histologically and genetically resemble the original tumors where they were derived since they are generated from patient/mouse-derived cancer cells or by engineering induced pluripotent stem cells [15,16]. Moreover, spheroids, and organoids have recently been used as promising platforms for preclinical research in personalized/precision medicine [17].

* Corresponding author. 585 Purdue Mall, West Lafayette, IN, 47907, USA.
E-mail address: bumsoo@purdue.edu (B. Han).

https://doi.org/10.1016/j.mtadv.2023.100408
Received 5 April 2023; Received in revised form 15 July 2023; Accepted 21 July 2023
Available online 2 August 2023

These engineered tumor models can generally provide a 3D microenvironment with cell-cell, cell-matrix, and cell-fluid interactions relevant to the tumor microenvironment (TME) *in vivo*. However, many of these models focus on tumor cells and often overlook the significance of the tumor-stroma interface, which is crucial to faithfully reconstitute the TME. Stroma tissue, consisting of primarily cancer-associated fibroblasts (CAFs) in a highly fibrotic extracellular matrix, interacts with tumor tissues in both biochemical and biomechanical ways and plays important roles in tumor progression, invasion, and drug resistance [15,18]. This suggests that the stromal component is critically important to create engineered tumor models representative of the TME *in vivo*. Thus, more recently developed 3D models, called assembloids, incorporate different cell types and enable spatial tissue organization [19–21]. Assembloids have been achieved by connecting or fusing organoids and spheroids resembling multiple cell/tissue types [22]. Later patient-specific tumor assembloids was reported comprising patient-derived bladder tumor tissue, CAFs, immune cells, and a muscle layer [23]. Several groups have also shown the concept of using spheroids/organoids as building blocks to form millimeter to centimeter-scale tissues at defined organizations [24,25].

However, there are still several key technical challenges to create tumor-stroma models capable of reconstituting native tumor-like environment. First, the cell density of the currently available tumor models is still significantly lower than that of native tissues. Cell packing density is crucially important to faithfully reconstitute cell-cell interaction at the tumor-stroma interface. The right cell packing density is also thought to closely relate to the mechanical status at this tissue-tissue interface. However, reaching a high cell density comparable to a native tissue (10^8–10^9 cells cm^{-3}) [26] requires a long culture duration using current techniques from the cell seeding density of typical 10^6 cells cm^{-3}. Achieving matured 3D tumor models with the highest cell density of 10^8 cells cm^{-3} compatible with native tumor tissues takes several days or weeks.

For example, the cell seeding density of the traditional methods of creating tumor spheroids/organoids is 10^5 cells cm^{-3}, and the growth of tumor cells into functional spheroids takes dozens of days [27,28]. Preparing tumor organoids is even longer since organoids are usually derived from stem cells and need specific differentiation [29,30]. The cell seeding density in the scaffold-based models is 10^6–10^7 cells cm^{-3}, and it takes a few weeks to obtain an engineered tissue with the highest cell density of 10^8 cells cm^{-3} [31,32]. Although the fabrication process is relatively faster for 3D bioprinting, the cell density of the bio-inks remains low (10^6 cells cm^{-3}) [33,34]. Consequently, the two practical limitations of current 3D tumor models are low cell seeding density and prolonged culture duration. Furthermore, there are few tumor models recapitulating mechanical stress status at the tumor-stroma interface. Although the significance of the biomechanics interactions at the tumor-stroma interaction is recognized [35,36], most tumor models are relying on co-culture with mechanically non-constraint cell-cell contacts. These models are not adequate to reconstitute the mechanical interaction at the tumor-stroma interface.

In this study, we report a new method capable of rapidly creating (<1 day) tumoroids with tumor-stroma interface at extremely high cell packing density (~10^8 cells cm^{-3}). This method, named as "inkjet-printed morphogenesis" (iPM), is based on a hypothesis that cancer cells and CAFs can exert differential contractile forces on the polymer matrix and actively compact the matrix. Thus, by inkjet printing of "two colors" cell-laden polymeric inks (i.e., cancer cells and CAFs), tumoroids with densely-packed cells will be formed by cell-derived compaction. The polymeric inks are prepared by mixing each cell line into interpenetrating-polymer inks (IPIs), formulated with Poly (N-isopropylacrylamide-*co*-acrylamide) P(NIPAM-*co*-AM), and type I collagen. First, the rapid formation of tumoroids by active shrinking is demonstrated and analyzed by time-lapse microscopy. Next, confocal microscopy and immunohistochemistry are conducted to characterize the cell density, detailed morphology, and specific biomarkers of printed tumoroids. Then, tumoroids' stiffness is measured by indentation tests to compare with murine tumors. Further iPM experiments are performed to investigate the force balance between cells' contractile force and the matrix resistance, to validate our hypothesis. Lastly, the concept of iPM is further extended to create complex cavity geometry and large tissue constructs. The results are discussed to establish a new method to rapidly create 3D tumor-stroma models that closely recapitulate the *in vivo* TME.

2. Materials and methods

2.1. Cells culture and reagents

Human pancreatic cancer cells (Panc10.05, labeled with tdTomato) and pancreatic cancer-associated fibroblast (CAF19, labeled with GFP) are primarily used. Panc10.05 and CAF19 are cultured in Dulbecco's Modified Eagle Medium (Advanced DMEM, Life Technologies, CA, USA) supplemented with 10% v/v fetal bovine serum (FBS), 2 mM L-glutamine (L-glu), and 100 μg ml^{-1} penicillin/streptomycin (P/S).

For testing the effect of cell type in this study, pairs of human prostate cancer cells (PC3) and prostate cancer-associated fibroblast (5286), and pairs of murine pancreatic cancer cells (KPC2) and murine cancer-associated fibroblast (mCAF) are also used. Human prostate cancer cells and the CAFs are cultured in the same medium as described above. The murine cancer cells and the CAFs are maintained in RPMI 1640 supplemented with 5% v/v FBS 2 mM L-glu, and 100 μg ml^{-1} P/S.

All cells were cultured in 25 cm^2 T-flask at 37 °C and 5% CO_2. Cells were harvested for the experiments using 0.05% trypsin and 0.53 mM EDTA (Life Technologies, CA, USA) when the cells reach 70–80% confluency.

2.2. Formulation of cell-laden interpenetrating-polymer inks (IPIS)

An interpenetrating-polymer ink (IPI) is formulated by mixing rat tail collagen type-I (Corning Inc., NY, USA) with Poly (N-isopropyl acrylamide-co-methyl methacrylate) (P(NIPAM-*co*-MMA)), Poly-SciTech, West Lafayette, IN). The inverse thermopolymers are selected due to their gelation kinetics can be controlled by varying the temperature. Furthermore, the ink can be formulated for relevant material properties for jetting and deposition. These properties are viscosity and surface tension. Besides, PNIPAM-based hydrogels and collagens are well-known ECM mimetic materials due to their high biocompatibility and biodegradability. Lastly, the addition of collagen is to add structural integrity, which provides physical support to tumoroids.

The P(NIPAM-co-MMA) is dissolved in deionized water at 4 °C to achieve 1% w/v concentration. A stock solution of rat tail collagen type-I is mixed with 10X PBS, 1 N NaOH, 0.1 M HEPE solution, 5% v/v FBS, 2 mM L-glu, 100 μg ml^{-1} P/S, and cell-culture grade distilled water at appropriate proportions to obtain a final collagen solution that had neutral pH, isotonic ionic strength, and a collagen concentration of 3 mg ml^{-1}. The IPI is then prepared by mixing 3 mg ml^{-1} collagen with 1% w/v P(NIPAM-co-MMA) with a 3:1 or 2:1 volume-to-volume ratio in the study to investigate the effect of polymer stiffness. Finally, cancer cell inks and CAF inks are prepared by mixing the IPI with harvested cancer cells and CAFs, respectively. The standard cell density of a cell-laden ink is 5×10^6 cells cm^{-3}. The cell densities of 10^5 and 10^6 cells cm^{-3} are prepared to investigate the effect of cell density. The drop volume upon printing is around a hundred nanoliters, so, there are around ten cells in a drop at a cell density of 10^5 cells cm^{-3} and a hundred cells at a cell density of 10^6 cells cm^{-3}.

2.3. Inkjet printing setup

The drop-on-demand (DOD) printing setup consists of a PipeJet dispenser (BioFluidiX, Germany) and a stage controller (Physik Instrumente, USA) [37].The PipeJet dispenser is driven by a tunable high

voltage pulse generated by the drop firing program and associated electronics. A piezo stack actuator driven by the high voltage pulse will extend and partially deform the tube/pipe installed in the dispenser. The deformation causes local volume change within the pipe that pushes a drop of ink/liquid out of the orifice/nozzle of the pipe. Cancer cell inks and CAF inks are supplied to the pipes from a connected ink reservoir above the dispenser. A pipe with a 500 μm diameter nozzle is used. An XY stage provides addressable substrate movement to 0.2 μm. Cell-laden ink drops with a diameter of ~1000 μm are deposited on a glass well-plate.

2.4. Inkjet printing of cell-laden interpenetrating-polymer inks (IPIS)

Prepared cancer cell ink and CAF ink are printed and cured using the inkjet printing setup. First, five cancer cell-laden drops are deposited on a glass well-plate, forming a line array. Then, the drops are cured for 1 min at 37 °C for gelation of IPI. Next, five CAF-laden drops are deposited adjacent to the first line and cured for 1 min at 37 °C for gelation of the whole structure. The cell medium is added afterward. Finally, the polymer matrix would be compacted by the contractile force generated by the cells. A 3D tumor-stroma model (i.e., tumoroid) will be formed as the matrix compacts. In addition, the tissue compaction process is recorded by time-lapse fluorescent microscopy (Olympus IX71, Japan).

2.5. Confocal microscopy

Before conducting confocal microscopy, cells in tumoroids are labeled for cell nuclei (Hoechst 33,342, Sigma Aldrich, MI). The stained tumoroids are fixed on day 3 with 4% formaldehyde for 10 min. Z-stacked confocal images are acquired at 10 μm intervals using a confocal microscope (A1R-MP, Nikon, Japan). At each focal plane, fluorescence illuminations are obtained. The fields of view of confocal fluorescence are reconstructed as 3D using ImageJ to highlight the configuration of the cells in 3D. Moreover, the nuclei signals at multiple stacks are used to count the cell number.

2.6. Preparation of mouse tumor

KPC tumor cell lines are generated from individual primary tumors derived from KPC ($Kras^{G12D/+}$, $p53^{R172H/+}$, $Elas^{CreER/+}$) mice at Purdue University Biological Evaluation Core. Cells are maintained in RPMI1640 medium containing 10% FBS and 1% penicillin/streptomycin. When cells are grown to about 70% confluency, they are lifted with 0.05% trypsin which is then neutralized via the addition of the medium containing 10% serum. Cells are washed 2×, and orthotopic injections of 50 μl are performed in C57 B l/6 mice at a concentration of 2×10^6 cells cm^{-3} in sterile PBS per mouse. Finally, the tumor tissue is harvested three weeks after injection.

2.7. Immunohistochemistry

Printed tumoroids are washed in PBS and fixed in 4% paraformaldehyde (PFA) for 10 min on day 3. Then, the fixed tumoroids are embedded in 4% low melting point agarose gel [38]. Next, it is subjected to routine histological processing. Finally, according to standard protocol, samples are paraffin-embedded, sectioned, and stained with H&E, Ki67, Vimentin, E-cadherin, and DAPI.

Mouse tumors are fixed in 10% neutral buffered formalin for up to 48 hr and are then placed in 70% ethanol. Next, samples are paraffin-embedded, sectioned, and stained with H&E according to standard protocol.

2.8. Indentation tests for characterization of elastic modulus

Normal indentation testing combined with a contact mechanics analysis is used to quantify the mechanical properties of the 3D printed tumoroids. A custom-built mechanical testing device is used to perform indentation experiments (Fig. 5 (A)). The device consists of a linearly encoded piezoelectric actuator (PI N-381 NEXACT) that controls motion and records displacement values, a 10 g capacity load cell (Futek LSB200 S-Beam) that records load values, and a cylindrical glass probe with 1 mm diameter (Edmund Optics). The setup has been described previously [39]. The flat end of the cylindrical probe compresses the spherical tumoroids (with ≈500 μm diameter) until reaching a pre-defined load of 500 μN, then retracts until the probe and tumoroid are no longer in contact. Additionally, these experiments are performed while the tumoroids are submerged underwater. The tumoroid tested is centered under the probe using a mechanical stage positioned over an inverted optical microscope (Leica DMi 8). Cyclic testing (n = 3) was first performed on a tumoroid to ensure that only elastic (reversible) deformation occurred during contact (see Fig. S2). Then, the load-displacement data recorded by the mechanical testing device is used to calculate the elastic modulus of the printed tumoroids by Hertzian contact mechanics theory (see supporting information).

Flat punch indentation testing was also used to determine the modulus of the mouse tumor. First, flat tumor slices with ~1 mm thickness are cut from bulk mouse tumors. Then, a punch with a 1 mm diameter is indented into the tumor until reaching a max compressive load of 1 mN and retracted. Finally, the load-displacement data recorded by the device is used to calculate the elastic modulus of the mouse tumor by using a common contact mechanics theory [40] (see supporting information).

2.9. Cell contraction assay

Each cell type is harvested, counted, and seeded in the interpenetrating polymer ink (IPI) with a cell density of 5×10^6 cells cm^{-3}. A cell-laden drop with 2 μl volume is pipetted in a glass well-plate. Then, the drop is cured at 37 °C for gelation of IPI. The culture medium is added afterward. Time-lapse images recording the contraction of cell-laden drop are taken for 24 h. Then, ImageJ software is used to measure the diameter of the drop. Finally, the contraction index is defined as the diameter changed at 24 hr versus the original diameter of the drop.

2.10. Statistical analysis

Relevant study groups in each experiment were compared using a paired *t*-test. A minimum of three samples were analyzed for each group. The minimum level for statistical significance was $p < 0.05$.

3. Results

3.1. Rapid formation of 3D tumor-stroma models by differential cell-derived contraction

Solid tumors are composed by heterogeneous cell population. Mainly, by cancer cells and stromal cells, embedded in extracellular matrix, all together forming the TME. Among the stromal cells, cancer-associated fibroblasts (CAFs) are the major cellular component of the tumor stroma which play an important role in matrix remodeling, secretion of cytokines and changing tumor stiffness by the accumulation of extracellular matrix components [41]. We hypothesize that the cancer cells and CAFs can exert contractile forces on the polymer matrix and CAFs exhibit stronger contractility than cancer cells, as illustrated in Fig. 1A. This hypothesized mechanism is accomplished by inkjet printing of cell-laden interpenetrating-polymer inks of P(NIPAM-AM) and collagen, as shown in the schematic process in Fig. 1B. First, cancer cell ink and CAF ink are printed and cured subsequently. Next, the culture medium is added. After adding the culture medium, the cell-embedded matrix will detach from the substrate and actively shrink due to the cells' contractile force. Finally, the cells with stronger contractility (CAF19) are anticipated to form in the inner side surrounded by the cancer cells

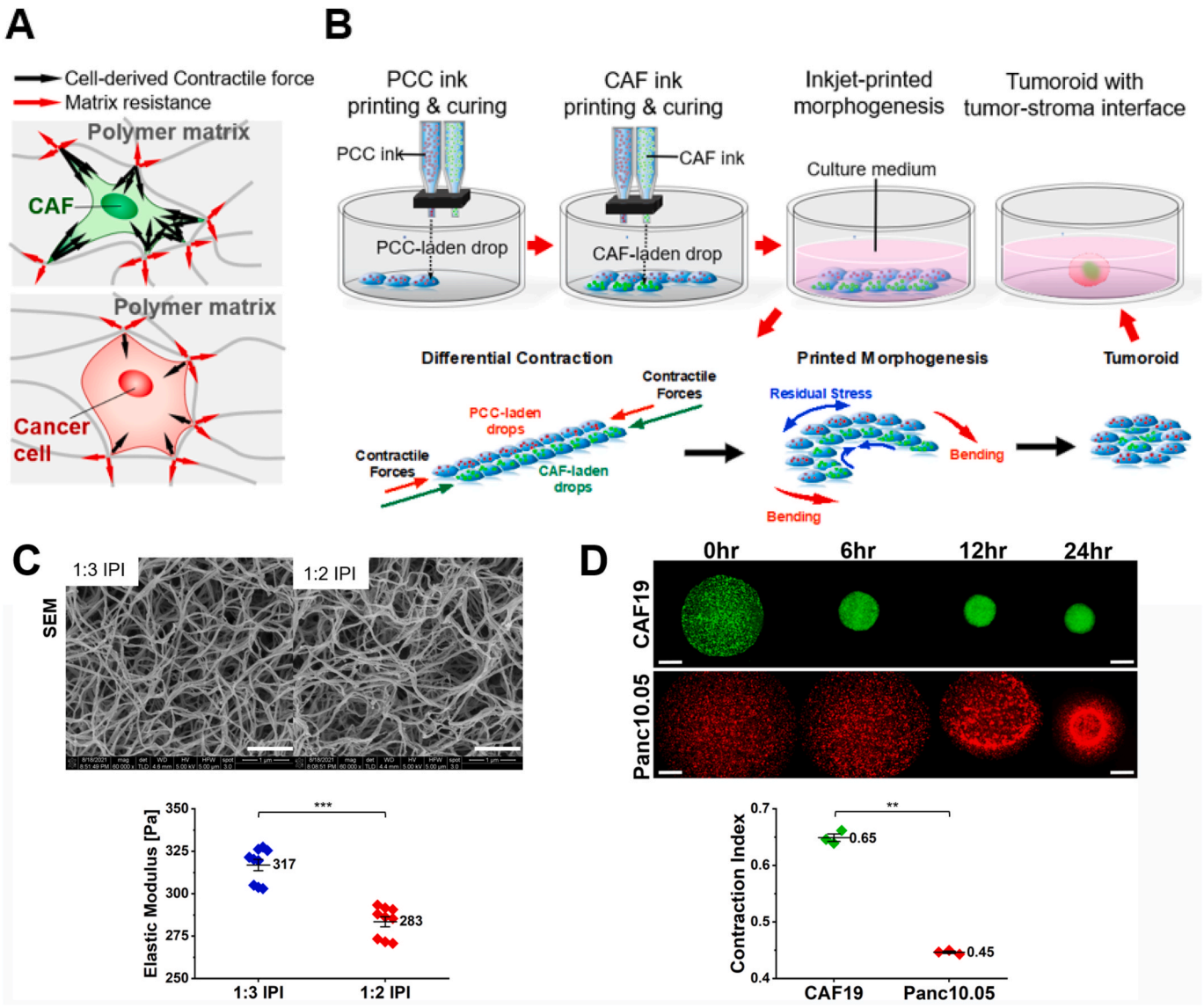

Fig. 1. The hypothesis of inkjet-printed morphogenesis of tumoroids. (A) Illustration of contractile forces generated by a CAF and a cancer cell on the polymer matrix; (B) Schematic of inkjet printing of cell-laden interpenetrating-polymer inks along with the hypothesized mechanism of tissue compaction; (C) Scanning Electron Microscopy (SEM) images showing the microstructures and the elastic modulus showing the mechanical stiffness of the interpenetrating-polymer inks (IPIs) (the ratio indicates the P(NIPAM-*co*-MMA) to collagen ratio) (scale bar: 1 μm); (D) contraction assay and quantification of contraction index of human pancreatic cancer cells (Panc10.05) and pancreatic cancer-associated fibroblasts (CAF19) (scale bar: 500 μm). ($n \geq 3$, *$p < 0.05$, **$p < 0.01$, ***$p < 0.001$).

with weaker contractility (Panc10.05). Moreover, we can note that residual stress exists within the tumoroids. The whole matrix is experiencing compressive stress; however, at the cancer cell-CAF interface, cancer cells are under compression, whereas CAFs are under tension with respect to their own tissue layer (illustrated by the blue arrows in Fig. 1B), allowing the bending of the two laden drops of each cell type. This captures a key feature of *in vivo* tumor microenvironment (TME): the tumor interior is experiencing compressive stress while the surrounding stromal tissue encounters tensile force [35,36,42]. To verify the stress distribution within the cell-laden matrix, a simple model mimicking the two-layer tissue compaction is performed by COMSOL Multiphysics provided in supporting information.

Fig. 1C shows the structural and mechanical characterization of the interpenetrating-polymer inks (IPIs) used in the study (see **Materials and Methods**). The ratio labeled in Fig. 1C suggests the P(NIPAM-co-MMA) to collagen volume-to-volume ratio. The result shows that IPI with more collagen (1:3 IPI) has a slightly higher stiffness but a less porous microstructure. In contrast, IPI with less collagen content (1:2 IPI) is softer and more porous. Furthermore, it is noted that although the inks are formulated with P(NIPAM-co-MMA) and type-I collagen, the fibrous structure of collagen dominates the microstructures of IPIs.

The contractility of the cells, namely human pancreatic cancer cells (Panc10.05) and the pancreatic cancer-associated fibroblasts (CAF19), is evaluated by contraction assay (see **Materials and Methods**) in Fig. 1D. The time-lapse images showing the contraction process of each cell type and the corresponding contraction index suggest that CAF19 is more contractile than the Panc10.05. This result is expected since studies have shown that fibroblasts are highly contractile and play an essential role in wound healing [43]. Also, chronic wound healing response by CAFs increased stiffness in the tumor by the accumulation of ECM proteins, which creates compressive forces [44].

3.2. Rapid formation and long-term culture of 3D tumoroids with tumor-stroma interface

As we showed before CAF19 are more contractile than Panc10.05,

then we test our hypothesis about the inkjet-printed morphogenesis. The fluorescent time-lapse images in Fig. 2A reveal the forming process in 24 hr, confirming that cells' contractile force compacts the matrix, and the mismatched strain determines the folding manner (see Movie S1 for the active shrinking process). Then, the volumetric strain was quantified by measuring the matrix area in the time-lapse images, as shown in Fig. 2B. The corresponding volumetric strain shows that the matrix size reduces significantly and that the 3D structure starts to be formed in 12 h. In addition, the created tumoroid exhibits a tumor-stroma interface with CAF19 (labeled with GFP - Green) inside and Panc10.05 (labeled with tdTomato - Red) outside, resulting from the contractility difference between cancer cells and CAFs, as shown in Fig. 2A at t = 24 hr. This confirms that the cells with higher contraction will self-assemble to the inner part of the tumoroid, whereas the cells with lower contraction will self-assemble on the exterior. The result shown confirms the differences in the cell's contractility can induce a shrinking process, that allows the formation of tumoroids with tumor-stroma interface.

This contraction also impacts the cell density and collagen concentration in the newly formed structures. The changes in cell density and collagen concentration are quantified based on the volumetric strain. The cell density increases rapidly with the rapid size decrease, as shown in Fig. 2C (blue curve). The predicted cell density of the 3D tumoroid on day 1 reaches 10^8 cells cm^{-3}, close to the cell density of native tumors [26]. However, the cell density might be underestimated since cell growth is neglected in the initial 24 hr of compaction. Similarly, the collagen concentration increases with the size decrease, as shown in Fig. 2C (red curve). The collagen concentration change serves as a conservative estimation since the collagen would degrade or be synthesized by the fibroblasts, which is not considered. Nonetheless, the quantification data provide a shred of evidence that the printed tumoroids have a composition with highly-packed cells and dense collagen content, close to the *in vivo* TME.

Moreover, the printed tumoroids could be cultured for at least two months, as demonstrated in Fig. 2D. During the two-months culture, the shape of the tumoroid remains uniform (sphere with 500 μm diameter). The average size of the tumoroids is consistent (note supporting information). Therefore, as the cells grow continuously in a confined space, the tumoroid becomes dense and experiences mechanical compressive stress within the structure. This environment replicates a key feature in actual tumors that total stress is compressive in the tumor's interior in all directions. In contrast, the tumor's periphery is experiencing compressive stress in the radial direction but tensile stress in the circumferential direction [35].

3.3. Microscopic and stiffness characterization of tumoroids by iPM

More details of the tumoroids were analyzed by confocal microscopy. Analysis of the images provides a more detailed morphology of the printed tumoroids. As shown in the 3D reconstruction in Fig. 3A, CAF19 cells are in the inner core of the tumoroid surrounded by cancer cells (Panc10.05). In addition, the result shown that CAF19 cells will grow extensively from the core to the surrounding, while cancer cells will grow homogeneously around the core of the CAFs. Furthermore, the cells' nuclei are visualized using the Hoechst staining (marked in blue). Fig. 3 B shows many nuclei signal at multiple z-stacks, allowing cell counting. Then, the tumoroid's volume is calculated by ImageJ based on the confocal image stacks. Finally, the measured cell density is 4.6×10^8 cells cm^{-3} (n = 3). This is significantly higher than those of conventional spheroids [27,28]. The high cell density of the printed tumoroids is again proved to be comparable to native tumor tissues and can more closely mimic the *in vivo* tumor microenvironment (TME).

The elastic modulus of the tumoroids was measured by indentation testing. The setup is shown in Fig. 3C, and the response of a tumoroid tested during loading and unloading is demonstrated in Fig. 3D (see Movie S2 for the indentation process). The tumoroid size increases with the probe's displacement due to the compression of the probe on the tumoroid. When the probe senses the prescribed maximum load, the tumoroid is experiencing a maximum compression and therefore has the

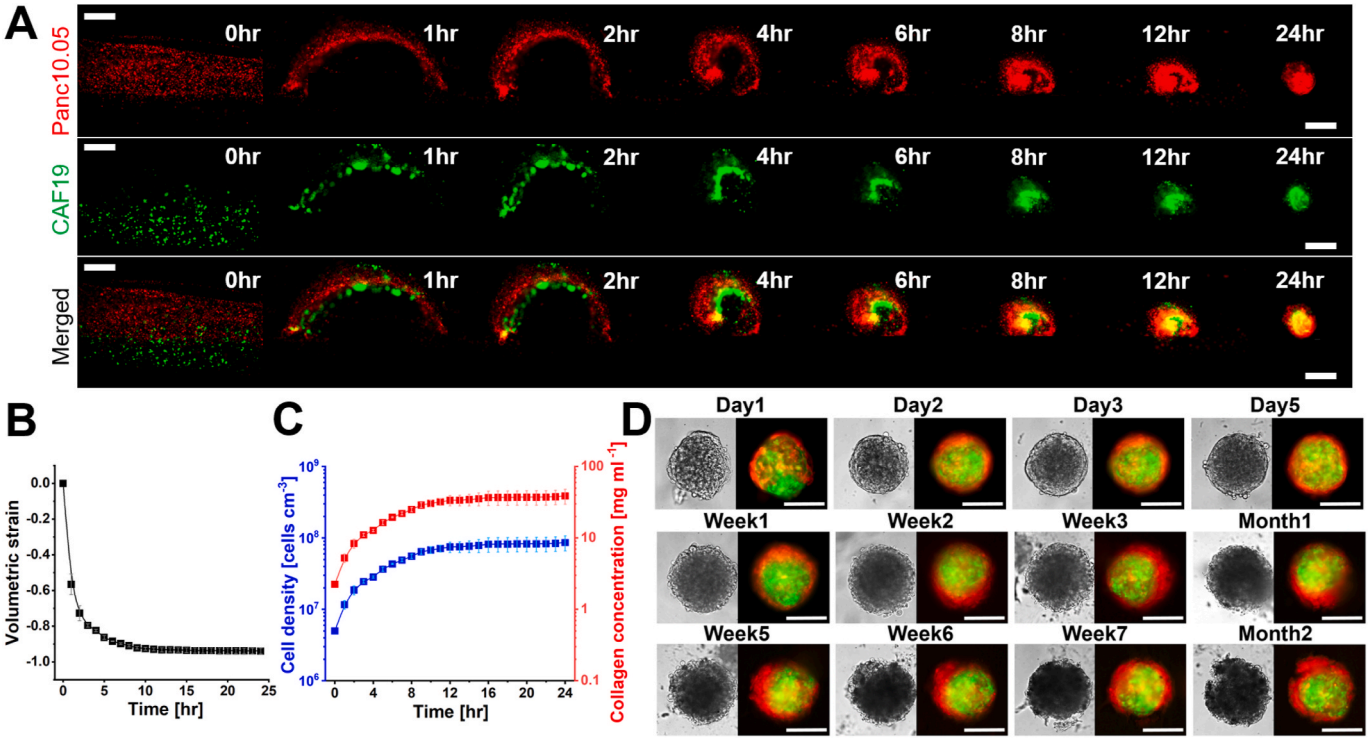

Fig. 2. Rapid creation of tumoroids by inkjet-printed morphogenesis. (A) 0–24 hr time-lapse images of active shrinking (red channel: Panc10.05, green channel: CAF19); (B) quantification of volumetric strain; (C) quantification of cell density and collagen concentration; (D) bright-field and fluorescent images of the different days of culture. (Scale bar: 500 μm). (For interpretation of the references to color in this figure legend, the reader is referred to the Web version of this article.)

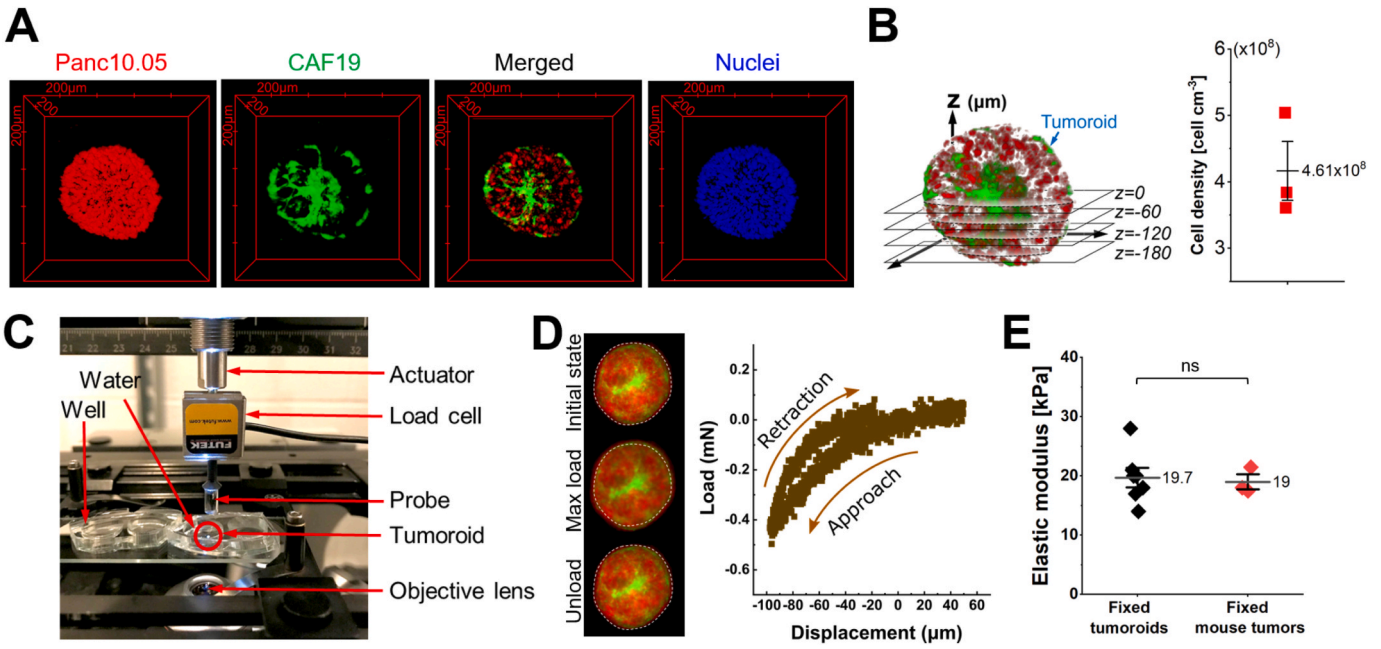

Fig. 3. Confocal microscopy analysis and elastic modulus measurement of tumoroids. (A) 3D reconstruction of Panc10.05, CAF19, overall structure, and nuclei by confocal microscopy; (B) schematic of image stacks at multiple z-depths, and the corresponding measured cell density; (C) photo of the indentation setup; (D) fluorescent images of the tumoroid at the initial state before loading, the maximum load, and the final state after unloading; and the displacement-load curves during loading & unloading of the tumoroid tested; (E) elastic modulus of fixed tumoroids and fixed tumors. ($n \geq 3$, *$p < 0.05$, **$p < 0.01$, ***$p < 0.001$).

largest size, as seen at "Max load" in Fig. 3D. Besides, we can observe that both CAFs and cancer cells deform by expanding radially outward upon compression. During unloading, the tumoroid size decreases and finally recovers to the original shape, as seen at "Unload," indicating an elastic deformation of the tumoroid. Furthermore, Fig. 3D shows the data acquisition from the device and the calculation of elastic modulus from the regression analysis. The plot presents raw load and displacement data acquired during indentation testing. These values had been corrected for compliance with the apparatus. Then, the elastic modulus of the tumoroid was determined by fitting theoretical load and displacement values to the experimental values gathered during testing, using the elastic modulus as a fitting parameter. The theoretical values were calculated using Hertzian contact mechanics theory [45] as previously shown by Briscoe et al. [46] (More details are provided in the supporting information). The fitting parameter that yields the best fit between the experimental and theoretical data (determined by a least-squares fitting method) is taken as the elastic modulus of the tumoroid.

We also performed indentation tests on the mouse tumor slices for comparison (see supporting information). Finally, the elastic modulus of fresh tumoroids, fixed tumoroids, and mouse tumors is obtained in Fig. 3E. Fixed tumoroids had a relatively larger modulus since studies have shown that a fixative is expected to harden tissue components and prevent decomposition, putrefaction, and autolysis [47]. Nonetheless, the modulus of printed tumoroids and actual mouse tumors share the same order of magnitude, suggesting the tumoroids created by our method have a comparable stiffness with native tumor tissues.

3.4. Phenotypic characterization of tumoroids formed by iPM

The phenotypic characterization of the printed tumoroids is attained by Hematoxylin and eosin (H&E) staining, immunofluorescence, and immunohistochemistry as shown in Fig. 4A. Hematoxylin stains the ribosomes, chromatin (genetic material) within the nucleus, and other structures as a deep blue-purple color. Eosin stains the cytoplasm, collagen, connective tissue, and other structures that surround and support the cell as an orange-pink-red color. H&E staining is performed on tumoroids to assess cell morphology and cellular arrangement. The stain shows the overall structure of the tumoroid with high cell density. Cells in the periphery of the tumoroid have small cytoplasm with a visible nucleus that resemble cancer cells. Mainly in the center it is observed a more intense pink color, it is also distributed all over the tumoroid that resembles CAF shape with big cytoplasm surrounded by collagen.

In order to determine the cell-cell interaction, the E-cadherin staining (green) was performed on the tumoroids, and nuclei were counterstained with DAPI (blue). E-cadherin expression confirms that the cancer cells being more outside the tumoroid but distributed across the whole structure, showing some interactions between cancer cells and CAF cells. Also, CAF cells were propagated into the tumor section and the tumor cells getting into the middle. So, there is no separate cancer cells and CAF growing in a 3D structure, it is more complex, the interaction between the cells occurs all over the tumoroid. Furthermore, the consistent and high E-cadherin expression suggests a solid cell-cell adhesion within the structure. This indicates that we can form functional tumor tissues instead of cell aggregates by using iPM. Additionally, the DAPI signal showing the nuclei of cells demonstrates that the tumoroid is constituted of highly-packed cells.

To analyze in depth the tumoroid, we also evaluated the Ki67 marker. Ki67 allows the evaluation of the proliferation status of a cell, and Vimentin, also known as intermediate fibroblast filament, are highly expressed in fibroblasts. Ki67 showed that the proliferative cells were mainly in the edge of the tumoroid and some of them inside the tumoroid to the mid-section, a zoom-in of the inset for the Ki67 expression is shown on the upper right of Fig. 4A. Furthermore, the expression of Ki67 is strongly associated with tumor cell proliferation and growth, implying the proliferation of the tumoroid. The expression of vimentin is mainly in the center but there are also positive vimentin cells near the edge of the tumoroid, suggesting the fibroblasts are present across the tumor but majorly organized in the core, a zoom-in of the inset for vimentin expression is shown on the bottom right of Fig. 4A. This confirms that there is an interaction between cancer cells and CAFs, the mixing between the cells occurs all over the tumoroid. These results show that the interaction between cancer cells and CAF not only

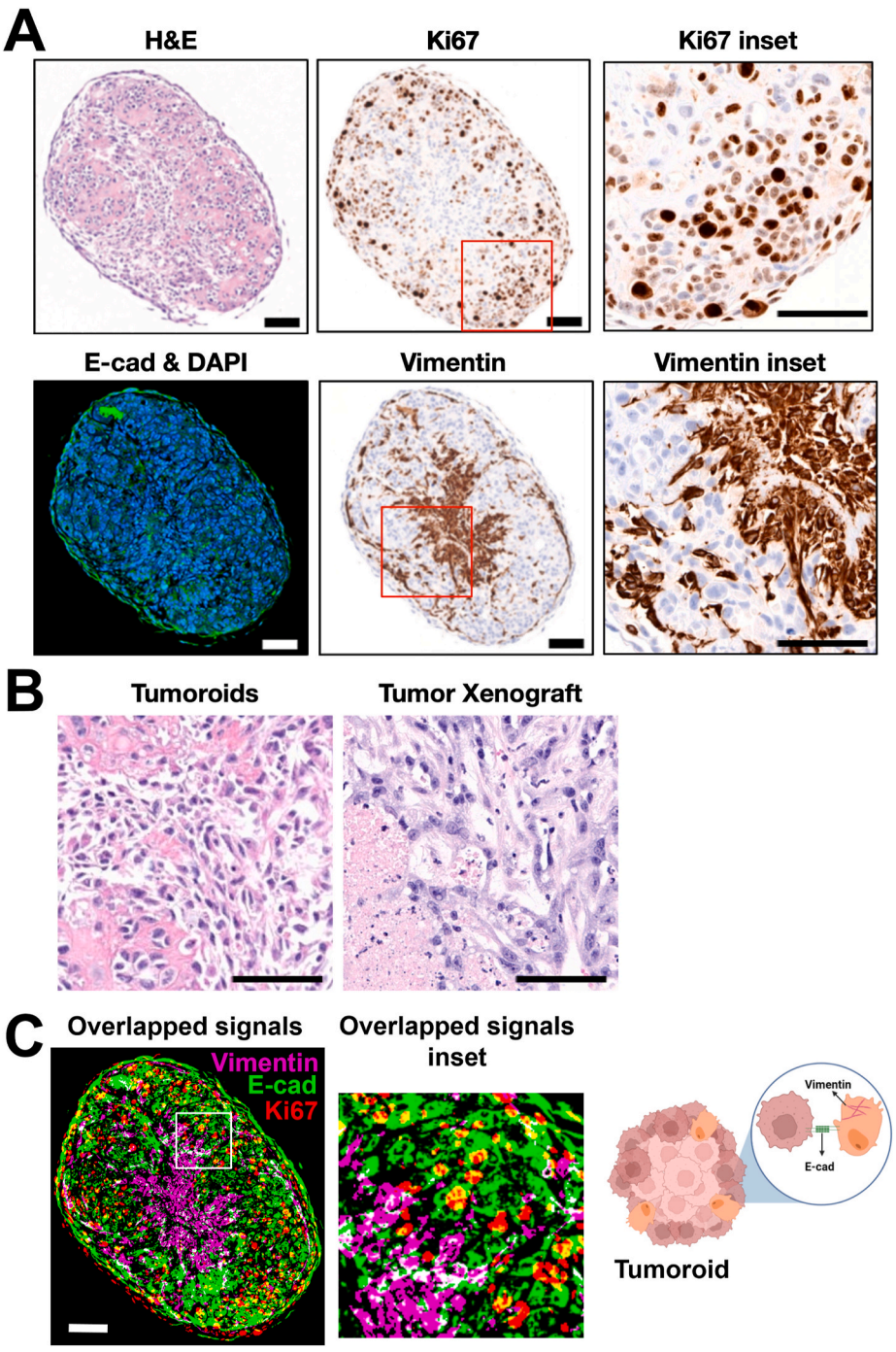

Fig. 4. Morphological and histological examination of the tumoroids. (A) Representative images of stained tumoroid with H&E, Ki67, vimentin, and E-cadherin & DAPI (corresponding zoom-in windows highlighted with the red square are shown on the right of each image); (B) Representative image of the stained tumoroid and the mouse tumor xenograft with H&E; (C) Overlapped expression of E-cadherin, vimentin, and Ki67 (corresponding zoom-in windows highlighted with the white square is shown on the right of the image). (Scale bar: 100 μm). (For interpretation of the references to color in this figure legend, the reader is referred to the Web version of this article.)

happens in the periphery, but also occurs in the center region of the tumoroid.

The distribution of cancer cells and CAFs strongly agree with the 3D reconstruction in Fig. 3A. In addition, Vimentin and Ki67 expression showed that the CAFs exhibit an elongated shape, and the cancer cells have rounded morphology.

The cellular density of the tumoroid is compared with xenograft tumors of the same cell type in Fig. 4B. It clearly demonstrates that tumoroids formed by iPM have comparable cell density of native tumors. Overall, the H&E staining demonstrates that the printed tumoroids closely recapitulate the *in vivo* TME, and the structure of native tumors.

The expression of Ki67, E-cadherin, and vimentin are further overlapped to identify the interaction between fibroblast and tumor cells, as shown in Fig. 4C. There are cells that express both Ki67 and E-cadherin, indicating the proliferating epithelial tumor cells. This happens near the periphery and the tumor-stroma interface. Interestingly, there are regions within tumoroid that cells express both E-cadherin and vimentin, mainly located at the tumor-stroma interface, as highlighted in the zoom-in inset in Fig. 4C. The tumoral cells could be in a transition from an epithelial phenotype to a more mesenchymal phenotype. The expression of E-cad in tandem with vimentin signals suggests that these cells could have a hybrid phenotype. Cells with hybrid phenotype can express epithelial and mesenchymal markers at once [48,49]. This hybrid phenotype at tumor-stroma interface may occur due to the crosstalk between the fibroblast and the tumoral cells. Recent studies have demonstrated that EMT can be promoted by biochemical and mechanical cues, like TGF-β, hypoxia and matrix stiffness [48]. For

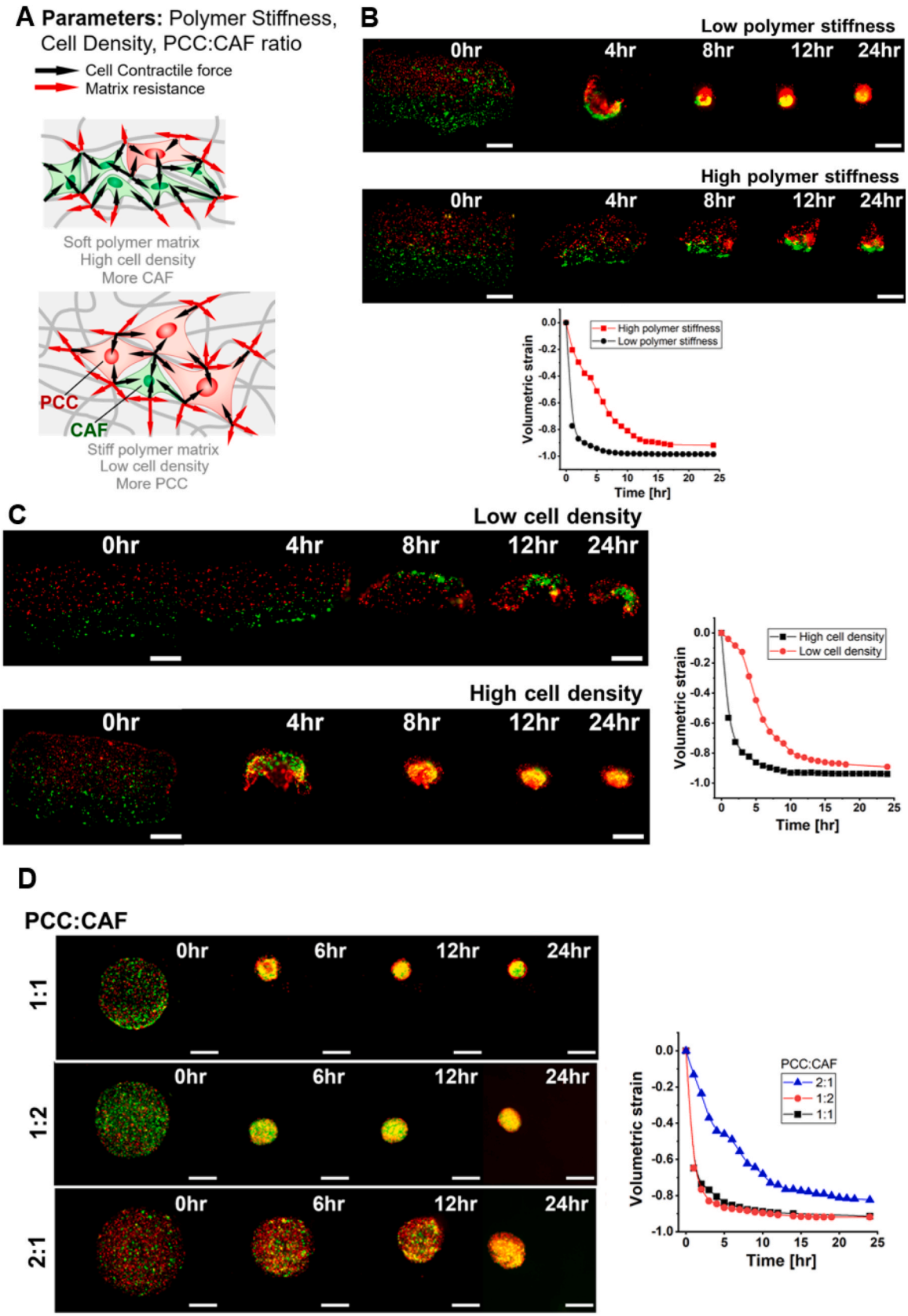

Fig. 5. Effects of the balance between cellular contractile force and matrix stiffness. (A) Schematic showing the effect of polymer stiffness, cell density, and cancer cell to CAF ratio. (B)Effect of polymer stiffness: 0–24hr time-lapse images of active shrinking at low and high polymer stiffness, and quantification of the volumetric strain at low and high polymer stiffness. (C) Effect of cell density: 0–24hr time-lapse images of active shrinking at low and high cell density, and quantification of volumetric strain at low and high cell density. (D) Effect of cancer cell to CAF ratio: 0–24hr time-lapse images of active shrinking, and the corresponding volumetric strains at 1:1, 1:2, and 2:1 cancer cell to CAF ratio (Scale bar: 500 μm).

PDAC many studies highlighted the presence of hybrid phenotypes on BxPc-3 and Panc-1 cell lines which co-express E-cad and vimentin [50, 51] specifically in the presence of hypoxia [52,53], when tumoral cells where co-culture with CAF [54] or because matrix stiffness [55]. Paracrine signaling plays an important role in the crosstalk between pancreatic tumoral cells and CAFs, it is well known that CAFs produce many growth factors like: inflammatory cytokines, chemokines, platelet-derived growth factor (PDGF), epidermal growth factor (EGF) and connective tissue growth factor (CTGF) [56]. CTGF plays a key role in the cell-stroma interaction. Specifically, CTGF is highly expressed by tumoral cells and CAFs in KPC cancer mouse model [57]. Other important signaling pathway is TGF-β which has an important role in EMT and mediates the crosstalk between CAFs and tumoral cells [58]. The printed tumoroid allows the interaction between the pancreatic cancer cells and CAFs which at the end is noticed by the presence of cells that co-express epithelial and mesenchymal traits. Therefore, the cells expressing vimentin might not only represent the fibroblasts but also post-EMT tumor cells.

3.5. Effects of force balance between cells and matrix

The compaction process is governed by the force balance between cells' contractile force and matrix resistance. Therefore, polymer stiffness, cell density, and the ratio of cancer cells to CAF cells are expected to be factors that regulate the matrix compaction. Specifically, the matrix will be compacted more at a softer matrix or with more cells of high contractility (i.e., higher cell density or more CAF), as illustrated in the upper figure in Fig. 5A. In contrast, stiffer polymer matrix, fewer cells or with lower contractility will impede the matrix compaction (note bottom figure in Fig. 5A).

The effect of the polymer stiffness was investigated by preparing interpenetrating-polymer inks (IPIs) with different stiffness. It is noted that the collagen concentration is constrained by both jetting and gelation behavior. The matrix won't be gelled if the polymer is too diluted (low stiffness), whereas the IPI cannot be ejected from the nozzle if the polymer is too viscous (high stiffness). Therefore, 3 mg ml^{-1} collagen was mixed with 1% w/v P(NIPAM-co-MMA) at 3:1 and 2:1 volume-to-volume ratios; and the final collagen concentration was 2.25 and 1.5 mg ml^{-1}, respectively. A collagen concentration of 2.25 mg ml^{-1} indicates a high polymer stiffness. On the other hand, 1.5 mg ml^{-1} collagen concentration represents a low polymer stiffness. As shown in Fig. 5B, the time-lapse images showing the tissue compaction and the corresponding volumetric strains at high and low polymer stiffness demonstrate that the matrix notably shrinks when cells are embedded in a softer polymer matrix. However, a stiffer matrix providing a stronger resistance slows down the cell-derived matrix compaction.

The effect of the cell density was examined by mixing the cells in IPI (2.5 mg ml^{-1} collagen concentration) at 10^5 and 10^6 cell cm^{-3} seeding density. The cell density of 10^6 cell cm^{-3} represents a higher seeding density, 10^5 cell cm^{-3} representing a low seeding density. Time-lapse images revealing matrix compaction and the corresponding volumetric strains. Fig. 5C show that decreasing cell density (low cell density) significantly hinders tissue compaction. In contrast, more cells (high cell density) generating a stronger contractile force enable rapid compaction.

Moreover, adjusting the contractile forces by changing the number of cancer cells and CAFs is also expected to influence the matrix compaction, as showed in Fig. 5A. To test this hypothesis, we mix the Pacn10.05 and CAF19 with a 1:1, 1:2, and 2:1 ratio and then print them in a single drop. The time-lapsed images in Fig. 5D show that increasing the CAF numbers (1:2) has no significant effect on tissue compaction but decreasing the CAF numbers (2:1) notably hinders the compaction. As a result, the difference in volumetric strains between the 1:2 (red line) and 1:1 (black line) ratios are negligible. However, reducing the CAF cells (blue line) impedes the compaction and affects the final tumor size on day 1. The results suggest that CAFs dominate the contraction, but a threshold amount of CAF is enough to compact the matrix significantly. In addition, time-lapse images in Fig. 5D demonstrates that the contractility difference between cancer cells and CAFs enables cell sorting. The cells of higher contractility (CAF19) are enveloped by the cells of lower contractility (Panc10.05) finally.

Overall, the results imply that the regulation of force balance between cells' contractile force and matrix resistance could potentially control the contraction to achieve the desired formation.

3.6. Tumoroids of various cell types formed by iPM

We hypothesize that the contractile force generated by cells drives the matrix compaction. Thus, the intrinsic contractility of different cell types is anticipated to affect the process. The effect of cell type on tissue compaction is assessed by applying various combinations of cancer cells and cancer associated fibroblasts to the proposed method. Mouse pancreatic cancer cells (KPC2) with mouse cancer-associated fibroblasts (mCAF) and human prostate cancer cells (PC3) with prostate cancer-associated fibroblasts (CAF5286) were used. First, to evaluate the contractility of each cell type, we perform the cell contraction assay, as described in the method section. Fig. 6A shows the contraction process of each cell type and the associated contraction index. Both mouse and human cancer cells (KPC2 and PC3) are less contractile than their associated fibroblasts (mCAF and CAF5286). The comparable contraction indices of mCAF (0.64) and CAF5286 (0.62) indicate that mouse and human fibroblasts have similar contractility in the interpenetrating-polymer matrix.

The time-lapse images showing the matrix compaction driven by different cell types are shown in Fig. 6B. The compaction processes differ from each other, which arises from intrinsic cells' behaviors. Nonetheless, CAFs of higher contraction organize in the center of the structure, while cancer cells with low contractility organize on the exterior. Moreover, the volumetric strains of both combinations are characterized in Fig. 6C. There is no significant difference in volumetric strain between cases since the contraction indices of all CAFs are similar (CAF19: 0.65, mCAF: 0.64, CAF5286: 0.62). The result suggests that CAFs dominate the tissue compaction regardless of the contractility of cancer cells. These results signify that the proposed method is applicable for different cell types as long as the cells have contractility, verifying our hypothesized mechanism. The cells' contractile forces exerted on the polymer matrix enable the matrix compaction and, finally, the formation of 3D tumoroids.

3.7. Layer-by-layer printing of tumoroids with cavity structure by 3d iPM

The inkjet printing of cell-laden interpenetrating-polymer inks (IPIs) can be further extended to create a more complex structure – a 3D cavity structure relevant to acinus shape. A three-layer configuration is printed to demonstrate the capability, as illustrated in Fig. 7A. The 3D geometry contains a bottom layer of 3 × 3 CAF19-laden drops, a middle layer of a Panc10.05-laden drop at the center, and a top layer of 3 × 3 CAF19-laden drops. The bottom layer is printed first, and the middle layer is printed afterward. Finally, the top layer was printed (see Movie S3).

Fig. 7B shows the matrix compaction after the 3D organization is printed at a 25 °C substrate. At 0 h, we observed that the Panc10.05-drop printed at the center spreads out on the bottom layer, caused by the IPI rehydration. Therefore, Panc10.05 cells (red) are transferred through the porous matrix to the periphery (as specified by the light blue dash arrows). After adding the medium, the matrix is compacted by the cells' contractile force, and the differential contractile forces govern the folding manner (see Movie S4 for the active shrinking process). We notice that the CAF19 of higher contractility dominates the tissue folding and eventually self-assembles at the center. On the other hand, the Panc10.05-laden matrix with lower contraction is driven by the CAF19-laden matrix and finally organizes in the peripheral region. Moreover, the folding direction is labeled with the white dash arrow at

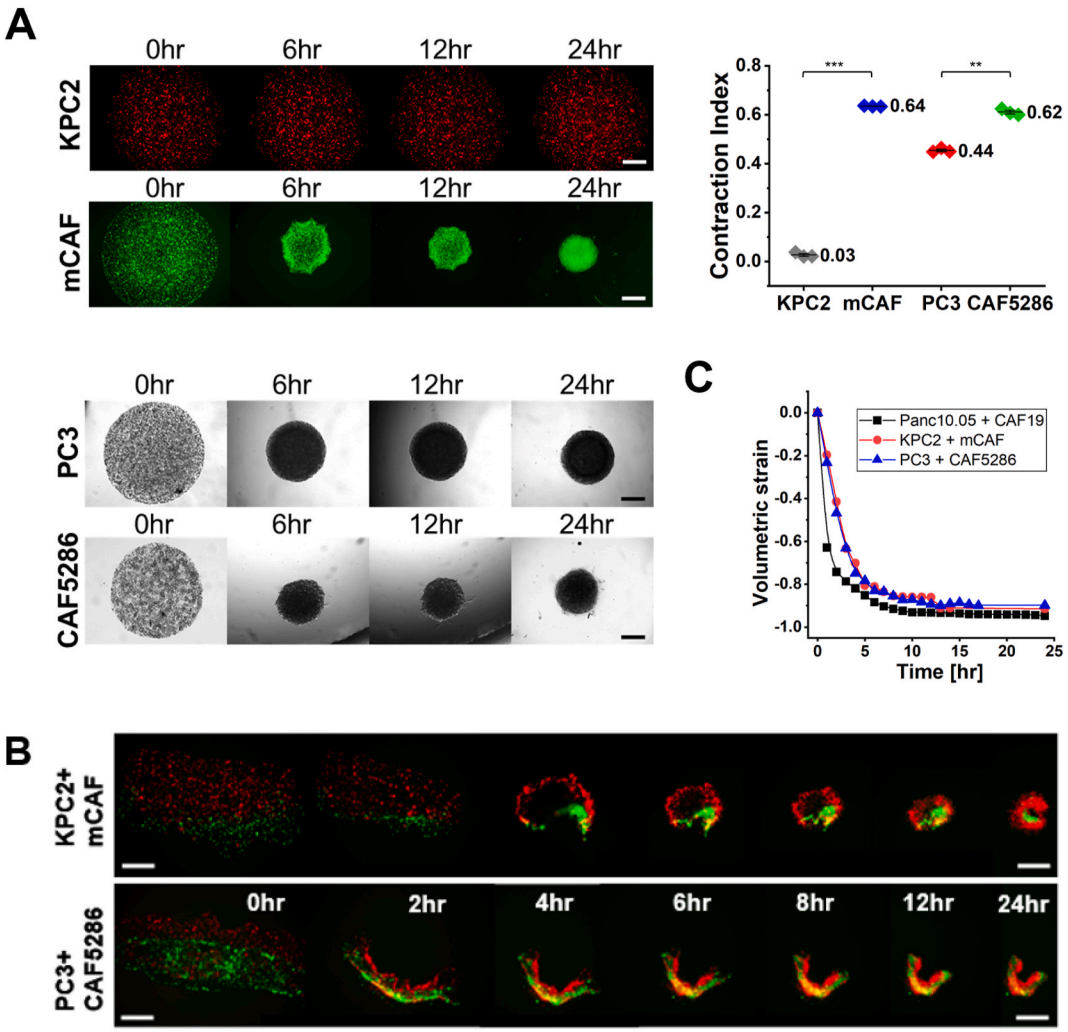

Fig. 6. Tumoroids from other types of cancer cells and CAFs. (A) Time-lapse images of tissue compaction of mouse pancreatic cancer cells (KPC2), mouse cancer-associated fibroblasts (mCAF), human prostate cancer cells (PC3), and human prostate cancer-associated fibroblasts (CAF5286); the corresponding contraction indices of KPC2, mCAF, PC3, and CAF5286 ($n = 3$, $^{*}p < 0.05$, $^{**}p < 0.01$, $^{***}p < 0.001$); (B) time-lapse images of active shrinking of KPC2 with mCAF, and PC3 with CAF5286; (C) quantification of volumetric strain. (Scale bar: 500 μm).

2 h. Compared with the previous line-pattern folding, the tissue folding with a surface interface represents tissue folding in a 3D manner, which resembles a 3D cavity shape. Nevertheless, the final tumoroid still possesses an organization with CAFs inside surrounded by cancer cells.

3.8. Creation of tumoroids with inner cancer cells-outer CAF configuration

To achieve the tumoroid configuration with cancer cells inside, CAF cells outside, two approaches are demonstrated. To better constrain the cell deposition during printing, we increase the substrate temperature to 35 °C to promote the gelation of IPI. As shown at 0 hr in Fig. 8A, Panc10.05 cells (marked in red) are well constrained at the center of the printed configuration. The polymer matrix becomes stiffer due to the elevated gelation that hinders tissue compaction. Time-lapse images exhibit a slow formation of tumoroid and CAF19 (marked in green) enclosing Panc10.05 (marked in red) during the process (see Movie S5 for the active shrinking process). In this case, the tissue compacts from all directions, as indicated by the white dash arrows at 6 hr.

Besides, more complex, and large-scale structures could be further achieved by the fusion of tumoroids. Studies have shown that tissue fusion is a fundamental biological process that is highly relevant to bio fabrication. When two or more spheroids/organoids/tumoroids make contact, they will coalesce over time to form one larger structure. As shown in Fig. 8B, the CAF tumoroids are placed at the surrounding of a cancer tumoroid. The cancer cells will finally be enclosed by CAF cells through the fusion process. The result shows that we could form a structure similar to the one formed by layer-by-layer printing on a 35 °C substrate by tissue fusion.

Moreover, the 3D reconstructions by confocal microscopy show a more detailed morphology of tumoroid with a structure in which CAFs surround cancer cells, as presented in Fig. 8C. Unlike the normal tumoroid, CAF19s cover the whole structure while the Panc10.05s are uniformly distributed at the structure's interior. Besides, the tumoroid is formed by a well-defined periphery of CAFs. Overall, the 3D reconstructions further demonstrate that we can achieve a tumor-stroma tumoroid with a configuration of cancer cells inside and CAFs outside by adjusting IPI's properties upon inkjet printing or by fusion of tumoroids.

4. Discussion

A wide variety of three-dimensional (3D) tumor models have been developed and have shown great potential to exhibit physiologically relevant cell-cell and cell-matrix interactions, heterogeneity, and structural complexity that replicate *in vivo* tumor microenvironment

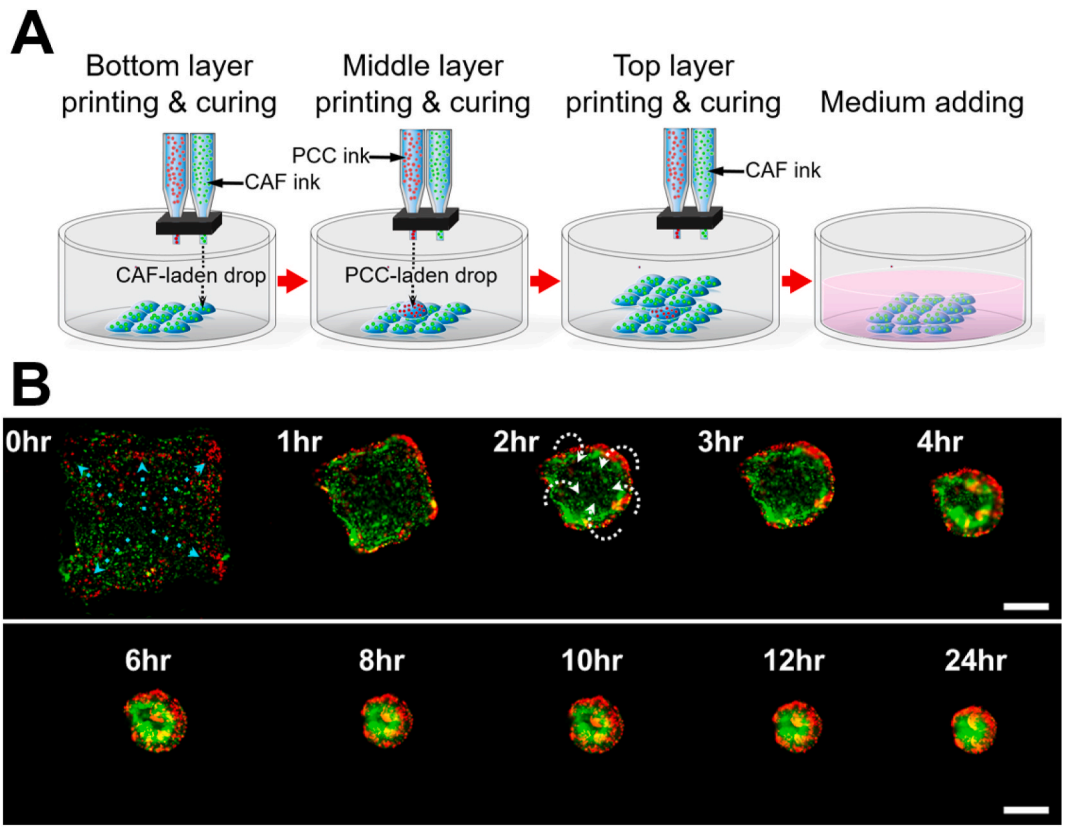

Fig. 7. Creation of tumoroids with 3D cavity shape. (A) Schematic of layer-by-layer printing of cell-laden IPIs. (B) Time-lapse images of active shrinking of 3D cavity shape after printed at a 25 °C substrate. (Scale bar: 500 μm).

(TME). However, some critical limitations of the existing 3D tumor models are low cell seeding density, low long-term culture, need of the addition of specific grow factors, and time-consuming preparation. In addition, due to the inherent differences in complexity and functionality, the choice of model usually depends on the application [59]. The current models lack reproducibility and a standardized protocol for any given cell type [60,61].

The iPM is a new method that allows 3D printing of tumoroids having many features of native tumors. With this method it is possible to create tumoroids with high cellular density, pre-design pattern and even structures with a complex cavity geometry. Here we printed tumoroids with cells embedded in collagen plus hydrogel which allows the interaction cell-cell, cell-matrix, and cell-medium that recapitulates better the cellular behavior *in vivo*. This method lets the formation of tumoroids composed by two key cells of native tumors. Here, the difference in the contractability of the cells enables the formation of the tumoroids where the shrinkage process is leading by CAFs. Previous studies have shown that the interaction between cells and ECM promotes cellular self-organization in matrices composed of collagen and hydrogel (4). Also, *in vivo* ECM is a dynamic environment that provides chemical and physical cues to the cells in it. In this context collagen plus hydrogel mimics the ECM located on tumors allowing the remodeling by the fibroblasts [62].

iPM also allows the formation of tumoroids in 1 day with a tumor-stroma interface at extremely high cell density (~10^8 cells cm-3), and collagen content. With this technique we used cell to cell interaction and cell to ECM interaction to generate a morphological change in the matrix that allow the formation of the tumoroid. Here, cancer associated fibroblast play a key role in the shrinkage and the organization of the cells in the tumoroid. Previous studies suggest that fibroblast in a 3D matrix interact physically with the microenvironment, through pushing and pulling. It has been shown that the traction force of fibroblasts changes collagen fibril arrangement, contraction and enhance the density [63]. A comparison between tumoroids and conventionally prepared spheroids was conducted to confirm the differences in the cell density between the tumoroids and conventional spheroids (see supporting information).

In addition, the printed tumoroids can be cultured for at least two months, demonstrating the potential for long-term culture, which is crucial for examining the long-term effects of TME, drug treatments at later-stage of disease [64,65], and tumor biology. The proposed method enables a large tumor size (~500 μm in diameter) compared to the spheroids or organoids prepared by the conventional techniques. A large tumoroid possesses an external proliferating zone and other aspects of the disease's pathophysiology. Large tumoroid size also enables an oxygen and nutrient gradient within the tumor, representing a key feature of *in vivo* TME. A hypoxia analysis on the tumoroid is provided in the supporting information, further demonstrating the presence of an oxygen gradient within the tumoroid.

Although a successful screening of drug efficacy is an ultimate goal of 3D tumor models, a related experiment wasn't conducted in the study since it should be designed considering both successful and failed drug candidate compounds. Unfortunately, pancreatic cancer, which is the focus of this manuscript, does not have any effective drugs. This results in an extremely low 5-year survival rate of 11%. Thus, no reliable drugs or drug candidates can be used to validate the 3D models. The developed 3D models may be better suited for cancer biology research to systematically study and identify potential therapeutic targets at tumor-stroma interactions.

Furthermore, a centimeter-scale tumoroid can be achieved by fusing multiple printed tumoroids. Many studies have attempted to use spheroids/organoids as building blocks to create large-scale tissues in a spatially controlled manner by patterning and fusion of spheroids/organoids [25,66,67]. These engineered tumor models of prescribed

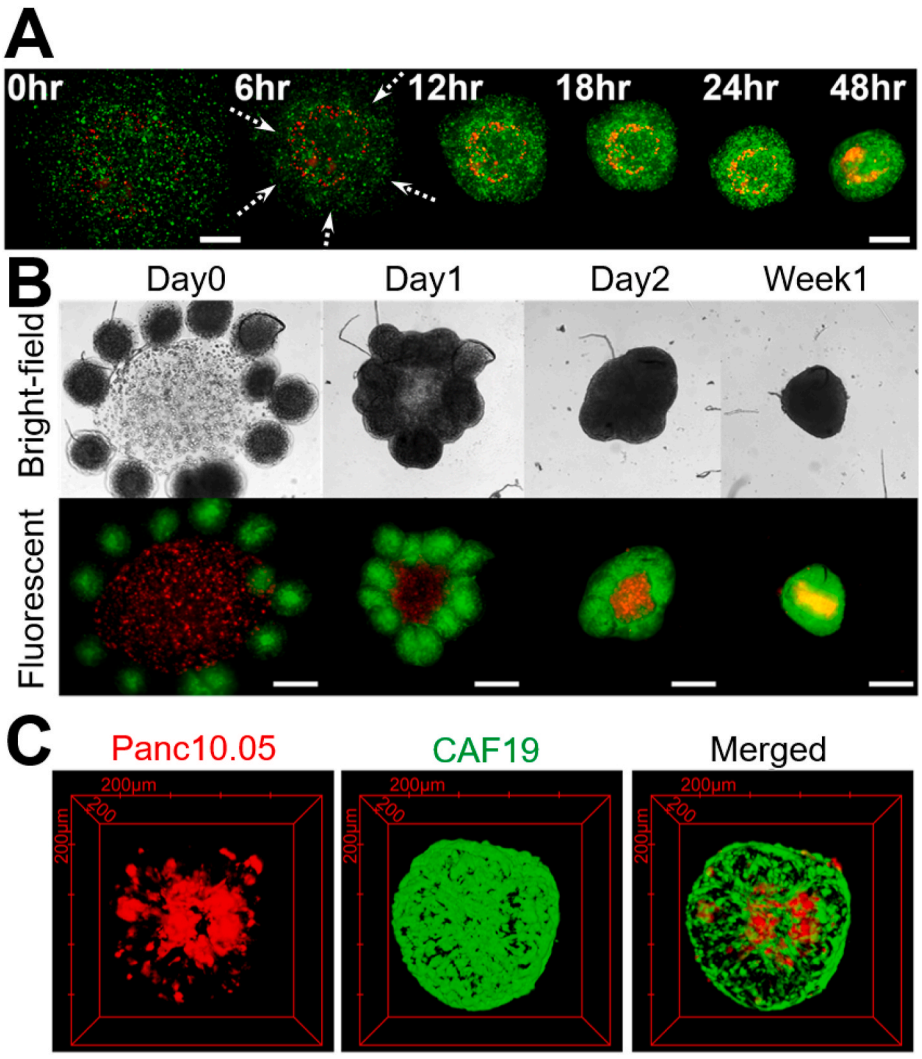

Fig. 8. Creation of tumoroids with inner cancer cells-outer CAF. (A) Time-lapse images of active shrinking of inner cancer cells-outer CAF configuration by layer-by-layer printing at a 35 °C substrate. (B) Bright-field and fluorescent images of fusion of tumoroids on Day 0, Day 1, Day 2, and week 1. (C) 3D reconstruction of Panc10.05, CAF19, and whole tumoroid by confocal microscopy. (Scale bar: 500 μm).

spatial organization could be a promising alternative for the tissue like constructs to mimic more closely the TME.

The presence of residual stress is a unique feature. At the cancer-CAF interface, cancer cells experience compression while CAFs are under tension, which is anticipated in the *in vivo* tumors. Although the CAFs are mainly located in the interior of the tumoroids, but not restricted to the center, here the tumor-stroma interface captures both biological and mechanical features of the TME. Also, 3D collagen matrices look like connective tissue environment, which is important to study cell behavior *in vitro* [68]. Lee; et al. shown that the stiffness in the matrix can modulate stem cell-like phenotypes of cancer cells, slight increase in the stiffness switching the cell phenotype to a more stem state of the cells [69]. That open a new question about the cells close to the periphery positive for vimentin. They are CAF cells or cancer cells that did the epithelial mesenchymal transition (EMT).

In addition, the iPM method were tested with various conditions (different collagen concentration), and various cell densities and types, which verifies the hypothesis that the active shrinking is governed by the force balance between cells' contractile force and matrix stiffness. Therefore, by adjusting the printing conditions, this study further demonstrates that the tumoroids with cancer cells organized at the center enveloped by the CAFs can be created. However, more precise control of the shrinking process is a crucial step that needs improvement to create the desired shape of tumoroids. As discussed, the mechanism is based on the force balance between the cell's contractile force and the matrix's stiffness. Here, CAF cells exert a force on the matrix that ends in the matrix contraction, by the cell shortening that produce an inward force [68]. Therefore, adding crosslinkers upon printing or substituting polymers might be solutions for adjusting the matrix's mechanical properties. Incorporating growth factors or varying cell density are approaches to regulating the cells' contractile force.

Overall, the results demonstrate that the proposed method provides a solution that can rapidly create 3D tumor models at extremely high cell density to address the limitations of existing models. Long-term culture ability, big size, highly-packed composition, and residual stress at the cancer-CAF interface closely recapitulate the *in vivo* TME. Besides, it is shown that the present method is generalizable and can be implemented with multiple types of cancer cells and CAF.

Furthermore, this method suggests a new concept of "digital cell printing" to create more complex structures and mechanical status beyond current 3D bioprinting techniques. The tumoroids created by the present method will be useful to construct a more reliable therapeutic screening platform for preclinical drug evaluation, drug delivery, tumor cell metabolism, signaling pathways, role of integrins and fibronectin. Integrins are key proteins in the interaction between cells and ECM [70], and fibronectin is a master organizer of the ECM [71]. Currently, *in vitro*

models for the analysis of new drugs are limited. Many of them focused only in 2D culture which does not resemble tumor complexity (TME) and the crosstalk between tumor cells. Numerous studies have been showed differences in drug response from cells, depending on culture type 2D or 3D (Tumoroids), suggesting that 3D culture could be more relevant for pre-clinical studies [72–75]. However, many studies that uses the 3D culture only evaluate the effects of the drugs in one cell type [76]. Tumoroids generated by iPM method will allow the evaluation of a drug in two different cell types (fibroblasts and tumoral cells) at the same time, and the effect of a key component of the ECM (here collagen).

5. Conclusions

We developed a novel inkjet-printed morphogenesis method using bi-cellular inks of collagen P(NIPAM-co-MMA) mixture to create tumor-stroma interface with extremely high cell density mimicking mechanical residual stresses at native tumors. We demonstrated that this method is applicable to other cell types and complex geometries by manipulating the force balance between cells and the matrices. This method opens new avenues for research on tumor biology *in vitro*.

Author contribution statement

Cih Cheng: Conceptualization, Investigation, Analysis, Writing-Original draft preparation, **Naomi Deneke:** Investigation, Analysis, Writing-Original draft preparation, **Hye-ran Moon:** Investigation, Analysis, Writing-Original draft preparation, **Sae Rome Choi:** Investigation, Analysis, Writing-Original draft preparation, **Natalia Ospina-Munoz:** Investigation, Analysis, Writing-Original draft preparation, **Bennett Elzey:** Analysis, Writing-Reviewing and Editing, **Chelsea Davis:** Analysis, Writing-Reviewing and Editing, **George Chiu:** Conceptualization, Analysis, Writing-Reviewing and Editing, **Bumsoo Han:** Conceptualization, Analysis, Writing-Reviewing and Editing.

Declaration of competing interest

The authors declare that they have no known competing financial interests or personal relationships that could have appeared to influence the work reported in this paper.

Data availability

Data will be made available on request.

Acknowledgments

This study was partially supported by grants from NIH (U01 HL143403, R01 CA254110, and U01 CA274304 to BH) and NSF (CMMI-1449358 to GC and MCB-2134603 to BH/GC), the Purdue University Institute for Cancer Research (P30 CA023168) and a Program Grant from Purdue Institute of Drug Discovery. The confocal microscopy images were obtained at the Purdue Imaging Facility at Bindley Bioscience Center.

Appendix A. Supplementary data

Supplementary data to this article can be found online at https://doi.org/10.1016/j.mtadv.2023.100408.

References

[1] A. Negro, T. Cherbuin, M.P. Lutolf, 3D inkjet printing of complex, cell-laden hydrogel structures, Sci. Rep. 8 (1) (2018), 17099.
[2] M. Rimann, U. Graf-Hausner, Synthetic 3D multicellular systems for drug development, Curr. Opin. Biotechnol. 23 (5) (2012) 803–809.
[3] S.R. Choi, Y. Yang, K.Y. Huang, H.J. Kong, M.J. Flick, B. Han, Engineering of biomaterials for tumor modeling, Mater Today Adv 8 (2020).
[4] K. Duval, H. Grover, L.H. Han, Y. Mou, A.F. Pegoraro, J. Fredberg, et al., Modeling physiological events in 2D vs. 3D cell culture, Physiology 32 (4) (2017) 266–277.
[5] L.J. Bray, D.W. Hutmacher, N. Bock, Addressing patient specificity in the engineering of tumor models, Front. Bioeng. Biotechnol. 7 (2019) 217.
[6] S. Chakraborty, T.J. DePalma, A. Skardal, Increasing accuracy of in vitro cancer models: engineering stromal complexity into tumor organoid platforms, Advanced NanoBiomed Research 1 (12) (2021), 2100061.
[7] M.E. Bregenzer, E.N. Horst, P. Mehta, C.M. Novak, S. Raghavan, C.S. Snyder, et al., Integrated cancer tissue engineering models for precision medicine, PLoS One 14 (5) (2019), e0216564.
[8] C. Wang, Z. Tang, Y. Zhao, R. Yao, L. Li, W. Sun, Three-dimensional in vitro cancer models: a short review, Biofabrication 6 (2) (2014), 022001.
[9] M.J. Bradney, S.M. Venis, Y. Yang, S.F. Konieczny, B. Han, A biomimetic tumor model of heterogeneous invasion in pancreatic ductal adenocarcinoma, Small 16 (10) (2020), e1905500.
[10] H.R. Moon, A. Ozcelikkale, Y. Yang, B.D. Elzey, S.F. Konieczny, B. Han, An engineered pancreatic cancer model with intra-tumoral heterogeneity of driver mutations, Lab Chip 20 (20) (2020) 3720–3732.
[11] X. Xu, M.C. Farach-Carson, X. Jia, Three-dimensional in vitro tumor models for cancer research and drug evaluation, Biotechnol. Adv. 32 (7) (2014) 1256–1268.
[12] M. Zanoni, M. Cortesi, A. Zamagni, C. Arienti, S. Pignatta, A. Tesei, Modeling neoplastic disease with spheroids and organoids, J. Hematol. Oncol. 13 (1) (2020) 97.
[13] S. Gunti, A.T.K. Hoke, K.P. Vu, N.R. London Jr., Organoid and spheroid tumor models: techniques and applications, Cancers 13 (4) (2021).
[14] B. Pinto, A.C. Henriques, P.M.A. Silva, H. Bousbaa, Three-dimensional spheroids as in vitro preclinical models for cancer research, Pharmaceutics 12 (12) (2020).
[15] J. Rodrigues, M.A. Heinrich, L.M. Teixeira, J. Prakash, 3D in vitro model (R) evolution: unveiling tumor-stroma interactions, Trends Cancer 7 (3) (2021) 249–264.
[16] K. Yuki, N. Cheng, M. Nakano, C.J. Kuo, Organoid models of tumor immunology, Trends Immunol. 41 (8) (2020) 652–664.
[17] Z. Gilazieva, A. Ponomarev, C. Rutland, A. Rizvanov, V. Solovyeva, Promising applications of tumor spheroids and organoids for personalized medicine, Cancers 12 (10) (2020).
[18] K. Pietras, A. Ostman, Hallmarks of cancer: interactions with the tumor stroma, Exp. Cell Res. 316 (8) (2010) 1324–1331.
[19] M. Mukhopadhyay, Assembling organs in vitro, Nat. Methods 18 (2) (2021) 119.
[20] N. Vogt, Assembloids. Nature Methods. 18 (1) (2021) 27.
[21] C. Schmidt, The rise of the assembloid, Nature (2021) S22–S23.
[22] F. Birey, J. Andersen, C.D. Makinson, S. Islam, W. Wei, N. Huber, et al., Assembly of functionally integrated human forebrain spheroids, Nature 545 (7652) (2017) 54–59.
[23] E. Kim, S. Choi, B. Kang, J. Kong, Y. Kim, W.H. Yoon, et al., Creation of bladder assembloids mimicking tissue regeneration and cancer, Nature 588 (7839) (2020) 664–669.
[24] J.A. Brassard, M. Nikolaev, T. Hübscher, M. Hofer, M.P. Lutolf, Recapitulating macro-scale tissue self-organization through organoid bioprinting, Nat. Mater. 20 (1) (2021) 22–29.
[25] A.C. Daly, M.D. Davidson, J.A. Burdick, 3D bioprinting of high cell-density heterogeneous tissue models through spheroid fusion within self-healing hydrogels, Nat. Commun. 12 (1) (2021) 753.
[26] U. Del Monte, Does the cell number 10(9) still really fit one gram of tumor tissue? Cell Cycle 8 (2009) 505–506. United States.
[27] S. Sant, P.A. Johnston, The production of 3D tumor spheroids for cancer drug discovery, Drug Discov. Today Technol. 23 (2017) 27–36.
[28] S. Raghavan, P. Mehta, E.N. Horst, M.R. Ward, K.R. Rowley, G. Mehta, Comparative analysis of tumor spheroid generation techniques for differential in vitro drug toxicity, Oncotarget 7 (13) (2016) 16948–16961.
[29] H. Xu, X. Lyu, M. Yi, W. Zhao, Y. Song, K. Wu, Organoid technology and applications in cancer research, J. Hematol. Oncol. 11 (1) (2018) 116.
[30] E.D. Wrenn, B.M. Moore, E. Greenwood, M. McBirney, K.J. Cheung, Optimal, large-scale propagation of mouse mammary tumor organoids, J. Mammary Gland Biol. Neoplasia 25 (4) (2020) 337–350.
[31] S. Talukdar, Q.T. Nguyen, A.C. Chen, R.L. Sah, S.C. Kundu, Effect of initial cell seeding density on 3D-engineered silk fibroin scaffolds for articular cartilage tissue engineering, Biomaterials 32 (34) (2011) 8927–8937.
[32] R. Tiruvannamalai-Annamalai, D.R. Armant, H.W. Matthew, A glycosaminoglycan based, modular tissue scaffold system for rapid assembly of perfusable, high cell density, engineered tissues, PLoS One 9 (1) (2014), e84287.
[33] M. Hospodiuk, M. Dey, D. Sosnoski, I.T. Ozbolat, The bioink: a comprehensive review on bioprintable materials, Biotechnol. Adv. 35 (2) (2017) 217–239.
[34] P. Datta, M. Dey, Z. Ataie, D. Unutmaz, I.T. Ozbolat, 3D bioprinting for reconstituting the cancer microenvironment, NPJ Precis Oncol 4 (2020) 18.
[35] R.K. Jain, J.D. Martin, T. Stylianopoulos, The role of mechanical forces in tumor growth and therapy, Annu. Rev. Biomed. Eng. 16 (2014) 321–346.
[36] J.M. Northcott, I.S. Dean, J.K. Mouw, V.M. Weaver, Feeling stress: the mechanics of cancer progression and aggression, Front. Cell Dev. Biol. 6 (2018) 17.
[37] C. Cheng, Y. Jae Moon, J.Y. Hwang, G.T. Chiu, B. Han, A scaling law of particle transport in inkjet-printed particle-laden polymeric drops, Int. J. Heat Mass Tran. (2022) 191.
[38] L.A. Wiley, D.C. Beebe, R.F. Mullins, E.M. Stone, B.A. Tucker, A method for sectioning and immunohistochemical analysis of stem cell-derived 3-D organoids, Curr Protoc Stem Cell Biol 37 (2016), 1c.19.1-1c..1.
[39] N. Deneke, A.L. Chau, C.S. Davis, Pressure tunable adhesion of rough elastomers, Soft Matter 17 (4) (2021) 863–869.

[40] K. Kendall, The adhesion and surface energy of elastic solids, J. Phys. D Appl. Phys. (1971) 1186–1195.
[41] N.M. Anderson, M.C. Simon, The tumor microenvironment, Curr. Biol. 30 (16) (2020). R921-r5.
[42] S. Torrino, T. Bertero, Metabo-reciprocity in cell mechanics: feeling the demands/feeding the demand, Trends Cell Biol. 32 (7) (2022) 624–636.
[43] J.P. Marquez, E.L. Elson, G.M. Genin, Whole cell mechanics of contractile fibroblasts: relations between effective cellular and extracellular matrix moduli, Philos Trans A Math Phys Eng Sci 368 (1912) (2010) 635–654.
[44] I. Jang, K.A. Beningo, Integrins, CAFs and mechanical forces in the progression of cancer, Cancers 11 (5) (2019).
[45] H. Hertz, The contact of elastic solids, J. für die Reine Angewandte Math. (Crelle's J.) 92 (1881) 156–171.
[46] B.J. Briscoe, K.K. Liu, D.R. Williams, Adhesive contact deformation of a single microelastomeric sphere, J. Colloid Interface Sci. (1998) 256–264.
[47] R. Thavarajah, V.K. Mudimbaimannar, J. Elizabeth, U.K. Rao, K. Ranganathan, Chemical and physical basics of routine formaldehyde fixation, J. Oral Maxillofac. Pathol. 16 (3) (2012) 400–405.
[48] M.K. Jolly, J.A. Somarelli, M. Sheth, A. Biddle, S.C. Tripathi, A.J. Armstrong, et al., Hybrid epithelial/mesenchymal phenotypes promote metastasis and therapy resistance across carcinomas, Pharmacol. Therapeut. 194 (2019) 161–184.
[49] V. Aggarwal, C.A. Montoya, V.S. Donnenberg, S. Sant, Interplay between tumor microenvironment and partial EMT as the driver of tumor progression, iScience 24 (2) (2021), 102113.
[50] Y. Gao, Z. Zhang, K. Li, L. Gong, Q. Yang, X. Huang, et al., Linc-DYNC2H1-4 promotes EMT and CSC phenotypes by acting as a sponge of miR-145 in pancreatic cancer cells, Cell Death Dis. 8 (7) (2017), e2924.
[51] M. Viotti, C. Wilson, M. McCleland, H. Koeppen, B. Haley, S. Jhunjhunwala, et al., SUV420H2 is an epigenetic regulator of epithelial/mesenchymal states in pancreatic cancer, J. Cell Biol. 217 (2) (2018) 763–777.
[52] H. Li, C. Peng, C. Zhu, S. Nie, X. Qian, Z. Shi, et al., Hypoxia promotes the metastasis of pancreatic cancer through regulating NOX4/KDM5A-mediated histone methylation modification changes in a HIF1A-independent manner, Clin. Epigenet. 13 (1) (2021) 18.
[53] M. Geyer, D. Schreyer, L.-M. Gaul, S. Pfeffer, C. Pilarsky, K. Queiroz, A microfluidic-based PDAC organoid system reveals the impact of hypoxia in response to treatment, Cell Death Discovery 9 (1) (2023) 20.
[54] J. Tao, G. Yang, W. Zhou, J. Qiu, G. Chen, W. Luo, et al., Targeting hypoxic tumor microenvironment in pancreatic cancer, J. Hematol. Oncol. 14 (1) (2021) 14.
[55] A.J. Rice, E. Cortes, D. Lachowski, B.C.H. Cheung, S.A. Karim, J.P. Morton, et al., Matrix stiffness induces epithelial–mesenchymal transition and promotes chemoresistance in pancreatic cancer cells, Oncogenesis 6 (7) (2017) e352–e.
[56] G. Biffi, D.A. Tuveson, Diversity and biology of cancer-associated fibroblasts, Physiol. Rev. 101 (1) (2021) 147–176.
[57] A. Neesse, K.K. Frese, T.E. Bapiro, T. Nakagawa, M.D. Sternlicht, T.W. Seeley, et al., CTGF antagonism with mAb FG-3019 enhances chemotherapy response without increasing drug delivery in murine ductal pancreas cancer, Proc. Natl. Acad. Sci. U. S. A. 110 (30) (2013) 12325–12330.
[58] F. Wu, J. Yang, J. Liu, Y. Wang, J. Mu, Q. Zeng, et al., Signaling pathways in cancer-associated fibroblasts and targeted therapy for cancer, Signal Transduct. Targeted Ther. 6 (1) (2021) 218.
[59] D. Lv, Z. Hu, L. Lu, H. Lu, X. Xu, Three-dimensional cell culture: a powerful tool in tumor research and drug discovery, Oncol. Lett. 14 (6) (2017) 6999–7010.
[60] B.L. LeSavage, R.A. Suhar, N. Broguiere, M.P. Lutolf, S.C. Heilshorn, Next-generation cancer organoids, Nat. Mater. 21 (2) (2022) 143–159.
[61] M. Vinci, S. Gowan, F. Boxall, L. Patterson, M. Zimmermann, W. Court, et al., Advances in establishment and analysis of three-dimensional tumor spheroid-based functional assays for target validation and drug evaluation, BMC Biol. 10 (2012) 29.
[62] A.M. Rosales, K.S. Anseth, The design of reversible hydrogels to capture extracellular matrix dynamics, Nat. Rev. Mater. 1 (2016).
[63] C. Guidry, F. Grinnell, Contraction of hydrated collagen gels by fibroblasts: evidence for two mechanisms by which collagen fibrils are stabilized, Collagen Relat. Res. 6 (6) (1987) 515–529.
[64] M.F. Estrada, S.P. Rebelo, E.J. Davies, M.T. Pinto, H. Pereira, V.E. Santo, et al., Modelling the tumour microenvironment in long-term microencapsulated 3D co-cultures recapitulates phenotypic features of disease progression, Biomaterials 78 (2016) 50–61.
[65] M. Cavo, D. Delle Cave, E. D'Amone, G. Gigli, E. Lonardo, L.L. Del Mercato, A synergic approach to enhance long-term culture and manipulation of MiaPaCa-2 pancreatic cancer spheroids, Sci. Rep. 10 (1) (2020), 10192.
[66] V. Mironov, R.P. Visconti, V. Kasyanov, G. Forgacs, C.J. Drake, R.R. Markwald, Organ printing: tissue spheroids as building blocks, Biomaterials 30 (12) (2009) 2164–2174.
[67] M.J. Susienka, B.T. Wilks, J.R. Morgan, Quantifying the kinetics and morphological changes of the fusion of spheroid building blocks, Biofabrication 8 (4) (2016), 045003.
[68] F. Grinnell, W.M. Petroll, Cell motility and mechanics in three-dimensional collagen matrices, Annu. Rev. Cell Dev. Biol. 26 (2010) 335–361.
[69] J. Lee, A.A. Abdeen, Y. Li, S. Goonetilleke, K.A. Kilian, Gradient and dynamic hydrogel materials to probe dynamics in cancer stem cell phenotypes, ACS Appl. Bio Mater. 4 (1) (2021) 711–720.
[70] J.A. Park, H.R. Lee, S.Y. Park, S. Jung, Self-organization of fibroblast-laden 3D collagen microstructures from inkjet-printed cell patterns, Adv Biosyst 4 (5) (2020), e1900280.
[71] J. Kaur, D.P. Reinhardt, Chapter 3 - extracellular matrix (ECM) molecules, in: A. Vishwakarma, P. Sharpe, S. Shi, M. Ramalingam (Eds.), Stem Cell Biology and Tissue Engineering in Dental Sciences, Academic Press, Boston, 2015, pp. 25–45.
[72] M. Azharuddin, K. Roberg, A.K. Dhara, M.V. Jain, P. Darcy, J. Hinkula, et al., Dissecting multi drug resistance in head and neck cancer cells using multicellular tumor spheroids, Sci. Rep. 9 (1) (2019), 20066.
[73] C. Yee, K.A. Dickson, M.N. Muntasir, Y. Ma, D.J. Marsh, Three-dimensional modelling of ovarian cancer: from cell lines to organoids for discovery and personalized medicine, Front. Bioeng. Biotechnol. 10 (2022), 836984.
[74] Y. Hirokawa, J. Clarke, M. Palmieri, T. Tan, D. Mouradov, S. Li, et al., Low-viscosity matrix suspension culture enables scalable analysis of patient-derived organoids and tumoroids from the large intestine, Commun Biol 4 (1) (2021) 1067.
[75] R. Augustine, S.N. Kalva, R. Ahmad, A.A. Zahid, S. Hasan, A. Nayeem, et al., 3D Bioprinted cancer models: revolutionizing personalized cancer therapy, Translational Oncology 14 (4) (2021), 101015.
[76] E. Sereti, I. Papapostolou, K. Dimas, Pancreatic cancer organoids: an emerging platform for precision medicine? Biomedicines 11 (3) (2023).